Comparative Analysis of Motors with Inner and Outer Reluctance Rotors and PM Stators

Oluwaseun A. Badewa, and Dan M. Ionel
SPARK Laboratory, Stanley and Karen Pigman College of Engineering, University of Kentucky, Lexington, KY, USA
o.badewa@uky.edu, dan.ionel@ieee.org

***Abstract*—This paper presents a comparison of special outer and inner reluctance rotor motor topologies with permanent magnet (PM) stators having toroidal AC windings. A systematic approach is taken to study and discuss the design geometries, the respective impact on performance, and adoption of technological advancements such as stator-only cooling and hair-pin winding for high slot fill factor. Parametric FEA models are developed for both topologies, and design of experiments (DoE)-based sensitivity analysis is used to study the effect of independent variables on specific performance metrics such as torque, motor loss, torque ripple, and power factor. Inner and outer rotor topologies are compared using the resulting Pareto fronts from multi-objective optimization. Optimized outer rotor designs using both non-rare earth PMs and ferrites are also investigated over selected drive cycles. The efficiency per cycle is evaluated at seven of the most representative points of the drive cycle obtained using a k-means clustering algorithm for the world harmonized light vehicle test procedure (WLTP), Orange County, and parcel truck (Baltimore) drive cycles.**

***Index Terms*—Electric vehicle, synchronous motor, Finite Element Analysis (FEA), non-rare earth PM, flux switching, hair-pin winding, sensitivity analysis, optimization, drive cycle analysis, k-means clustering algorithm.**

I. Introduction

The use of electric vehicles (EVs) is on the increase in the world's largest countries including the US. The growth in EVs can be attributed to government support incentives, energy savings, increasing global emphasis on sustainability, and a growing desire to mitigate greenhouse gas (GHG) emissions [1]. Also, rapid advancements in power train development, energy storage components, and fast charging systems are some example developments enabling high global growth in EV adoption [2].

Recently, Severson *et al.* [3] estimated that 80 - 90% of existing EV traction motors use rare-earth PMs due to their high coercivity, thermal properties, and high maximum energy product (B-H)max. Limitations in the supply of rare-earth magnets have motivated the development and application of new innovative PM materials, such as Niron, non-rare earth PMs, and totally magnet-free EV traction motor designs as described in the works of Al-Qarni *et al.* [4], Luk *et al.* [5], and Badewa *et al.* [6], [7] to ensure long-term sustainability. To maximize PM usage, concepts such as those of PM flux concentration which has been previously applied for IPM spoke-type rotors and earlier demonstrated on research and industrial development projects, e.g. [8], [9] are applicable.

Profiled wires, such as flat or rectangular shaped variants, are a technology under development for significantly higher slot fill factor than traditional round wire. As reported in the works of Tom *et al.* [10], Kampker *et al.* [11], and Selema *et al.* [12], the use of flat and rectangular wires in rectangular slots can achieve high slot fill factors (≥ 0.7), and are adaptable to latest technologies such as stacked continuous hair-pin winding technology, additive manufacturing, laser marking, and 3D printing.

Demagnetization risks due to elevated operating temperatures resulting from losses pose a significant challenge in PM motors. Innovative cooling methods are therefore being constantly sought out, for example, those recorded in the works of Konovalov *et al.* [13], Sixel *et al.* [14], and Simpson *et al.* [15], to manage thermal stresses, maintain optimal operating temperatures, preserve magnet integrity, and ensure motor reliability.

Due to the volumetric and gravimetric restrictions in vehicles, despite advancing technology, compactness and high power density remain typical goals for EV applications with continuous efforts towards achieving these goals as documented in works of Fatemi *et al.* [16], and Han *et al.* [17]. The current paper extends the concept of PM flux concentration, this time for synchronous machines with stator excitation, sometimes referred to in recent literature as being of the flux switching type. The performance impacts of geometrical choices in inner and outer rotor electric machine topologies are studied and large-scale multi-objective optimization employing differential evolution (DE) is used to obtain optimal designs with 20 and 28 magnetic poles for comparison in terms of specific torque and power density [18]. Also, the performance of an optimized outer rotor motor design employing ferrites is analyzed for selected light-duty EV drive cycles.

II. Topologies and Specific Aspects

A. Principle of Operation

The combination of AC toroidal coils, spoke-type PMs, and castellated rotors in inner and outer configurations as shown in Figs. 1 and 2 respectively, allows for operation based on the reluctance principle, and flux concentration likely only for the outer rotor topology. The working mechanism, explained using the airgap modulation theory and parametric analyses, has been previously reported in greater detail in the works of Han. *et al.* [17], and Badewa *et al.* [6].

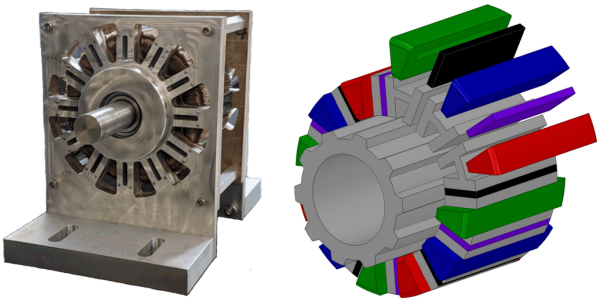

Fig. 1. Open Frame Lab Prototype (OFLP) and 3D solid model of the existing high power density motor using a castellated inner rotor and a modular stator with PMs and AC 3-phase windings.

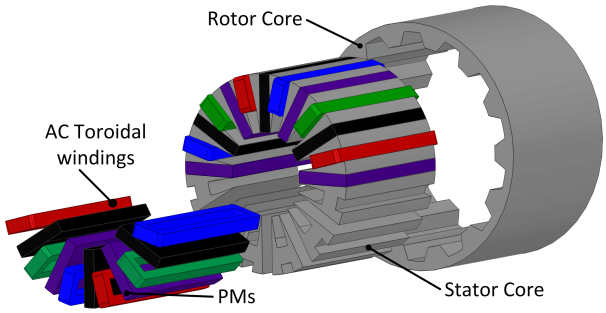

Fig. 2. Exploded view of the proposed 10″ OD outer rotor motor with stator concentrated coils and tangentially magnetized PMs. Both rare-earth PM and ferrite designs are studied.

The overall modulated MMF $F_{mod}(\theta, t)$ in the proposed machines is generated by the PM and armature fields, modulated by stator and rotor, and can be expressed as:

$$F_{mod}(\theta, t) = F_{PM}(\theta) + F_{aw}(\theta, t), \tag{1}$$

where F_{PM} and F_{aw} are the modulated MMFs of the PM and armature fields respectively, which are functions of position, θ, and time, t.

The electromagnetic torque, T_e, can then be derived as:

$$T_e = \frac{D_g^2 \ell_{stk}}{4\mu_0} \int_0^{2\pi} F_{mod}(\theta, t)\Lambda_r(\theta, t)\, d\theta, \tag{2}$$

where D_g is the airgap diameter, ℓ_{stk} is the stack length, and $\Lambda_r(\theta, t)$ is the rotor permeance function. For increased accuracy, all torque computations are done using FEA employing the Ansys Electronics 2023 software [19].

B. Rotor Geometry

For most electric machines, the airgap diameter, D_g, has been found to have a direct impact on the torque produced as described in the works of Murataliyev *et al.* [20], and Lehr *et al.* [21], such that:

$$T_e \propto (D_g)^2. \tag{3}$$

The outer rotor topology has the advantage of having a larger airgap diameter, and therefore higher torque than an inner rotor configuration.

The number of pole pairs, which corresponds to number of rotor protrusions, N_{pr}, also has a large impact on the resulting torque, power density, and efficiency as documented in the works of Han *et al.* [17], and Anvari *et al.* [22]. In both the outer and inner rotor topologies, larger values of N_{pr} are desirable with due consideration to the resulting switching frequency, core loss, and power electronics.

C. Flux Concentration Capability

The spoke-type arrangement of PMs in the stator enables flux intensification which can be quantified by a flux concentration ratio, ξ, as described in [6], [23], such that:

$$\xi = \frac{2h_{PM}}{\tau_p}, \tag{4}$$

where, h_{PM} is the PM height along the rotor radius, and τ_p is the stator pole pitch, i.e., stator outer circumference πD_s divided by the number of PMs, n_{PM}.

The capability for flux concentration is greatly limited in the inner rotor topology because the height of the PMs is restricted by the rotor. In contrast, in the outer rotor topology, the spoke-type PMs can be extended farther radially inward, thus achieving higher flux concentration. This extension of the PM length in the outer rotor topology provides a distinct advantage such that cheaper non-rare earth and lower remanence PMs such as ferrites [24] and innovative materials, for example, iron nitride PMs [4], [25] can be used to achieve high flux concentration and competitive performance with designs using rare-earth PMs.

D. Slot Shape and Stator Tooth

The stator slot shape affects the size of the stator tooth and the maximum achievable slot fill factor. Utilization of a trapezoidal slot for the inner rotor topology allows for more steel in the stator tooth due to the tapered edge in the smaller inner diameter as shown within the red-dotted area in Fig. 3.

In the outer rotor topology, the rectangular slots allow for large steel area in the stator tooth as the rotor interacts with the larger outer diameter of the stator. These rectangular slots are more suited for modern hair-pin winding technology using flat/rectangular wires which has been proven to be capable of achieving high slot fill factors in the range of 0.7 as described by Masoumi *et al.* [26].

Both the inner and outer rotor topologies feature open slots in which the winding conductors may exposed to relatively large variations of the magnetic field. This may lead to eddy currents and supplementary losses, which may be calculated using special analytical and FEA based methods, such as those proposed and described for example in [27], [28]. In the electric machines discussed in this paper, reducing the slot-opening, a common mitigation method for reducing eddy current may result in a reduction of the electromagnetic torque, and hence other techniques such as employing Litz wire may be considered [29].

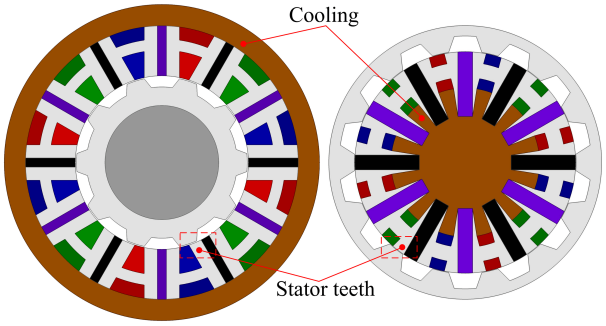

Fig. 3. Cross-sectional views of the inner and outer rotor motor designs illustrating in brown possible implementations of cooling, and different stator slot shapes.

E. Integrated Cooling

In the inner rotor topology, having moved all the active components to the stator, the typically implemented cooling method as described in [30] is either with an external structure such as a cooling jacket wrapped around the stator as described by Gai *et al.* [31], or an air heat-exchanger with cooling fins and embedded pipes as described as described by Konovalov *et al.* [13]. These cooling structures result in a volumetric increase as shown in Fig. 3.

In the outer rotor topology, it is proposed that with advanced cooling techniques, the cooling structure can be embedded within the stator. This results in a limited increase in the overall volume of the machine and a more compact design.

III. Multi-objective Optimization including Drive Cycle Analysis

Design of experiments (DoE)-based sensitivity analysis employing central composite design and non-linear regression methods has been used to show the influence of geometrical independent variables on motor performance [18], [32]. The parametric model of the inner and outer rotor topologies have eight and eleven independent geometrical variables respectively as shown in Fig. 4, and their influence on performance is studied in a comparative manner using results from FEA employing the Ansys Electronics 2023 software [19] as shown in Figs. 5 and 6. Additionally, the effect of the airgap length, g, was studied in the outer rotor design and showed that the minimum is always desirable in line with expectations.

Parametric models of outer rotor designs with 10 and 14 rotor protrusions employing N42UH NdFeB rare-earth PM were optimized with a fixed outermost diameter of 173mm and objective power density of 50kW/L as previously optimized inner rotor designs for comparison [17]. Multi-objective optimization combining DE and FEA was employed to maximize power density and power factor while minimizing motor losses at 12,500rpm. Optimal ranges were preset for the independent geometric variables as summarized in Tables I and II and shown in Fig. 4 based on systematic studies of the design space to ensure a broad optimization area and production of robust and mechanically stable designs [18], [33]. The Pareto fronts obtained from the optimization of the outer rotor topology

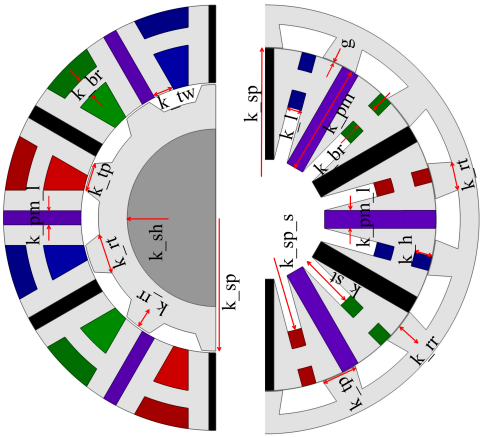

Fig. 4. Cross-sectional view of inner and outer rotor designs with labeled geometric independent variables considered in the multi-objective optimization.

Table I
Independent variables for the inner rotor design optimization, and their ranges.

Variable	Description	Min	Max
k_sp	split ratio	0.48	0.72
k_pm_l	PM width ratio	0.20	0.30
k_br	bridge length ratio	0.20	0.30
k_tw	stator tooth width ratio	0.20	0.30
k_sh	shaft dia. ratio	0.56	0.84
k_tp	rotor pole top ratio	0.48	0.72
k_rt	rotor pole root ratio	0.40	0.60
k_rr	rotor pole depth ratio	0.24	0.36

Table II
Independent variables for the outer rotor design optimization, and their ranges.

Variable	Description	Min	Max
k_sp	split ratio	0.80	0.90
k_pm	PM length ratio	1.00	1.20
k_pm_l	PM width ratio	0.18	0.30
k_br	bridge length ratio	0.40	0.50
k_h	slot length ratio	0.40	0.60
k_l	slot width ratio	0.40	0.60
k_tp	rotor pole top ratio	0.30	0.50
k_rt	rotor pole root ratio	0.30	0.50
k_rr	rotor pole depth ratio	0.40	0.60
k_sp_s	stator split ratio	0.40	0.50
k_st	stator extension ratio	0.25	0.35

are presented in Fig. 7, and comparison of these designs with optimized inner rotor designs is as shown in Fig. 8.

The efficiency per cycle is a metric for motor performance over a drive cycle, and a method for approximating this is by computing over the most representative points otherwise known as centroids of the drive cycle. These centroids are torque-speed points in the drive cycle that have the highest energy weights such that they are the most critical points at which a motor should perform best as investigated by Fatemi *et al.* [16] and shown in Fig. 9.

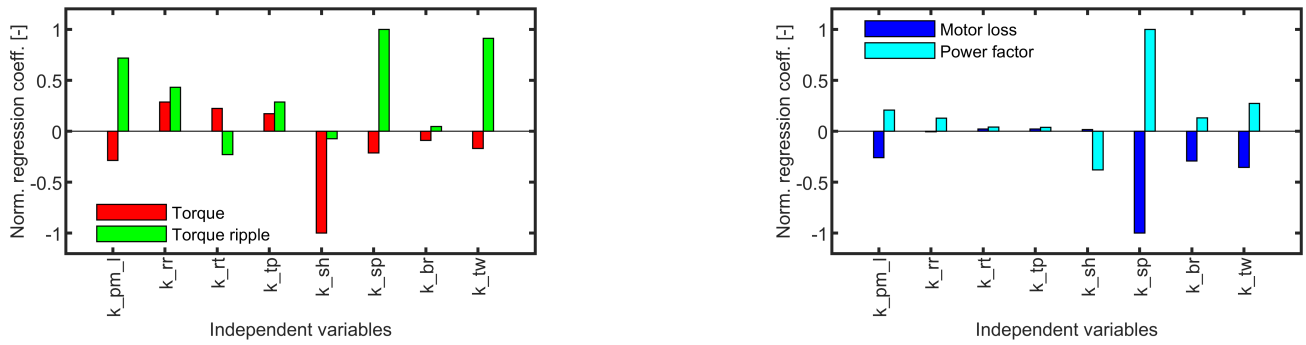

Fig. 5. Normalized non-linear regression coefficients for inner rotor motor configuration showing influence of independent variables on (a) torque and torque ripple, (b) motor loss and power factor, with the split ratio k_{sp} having considerable influence on the studied performance metrics.

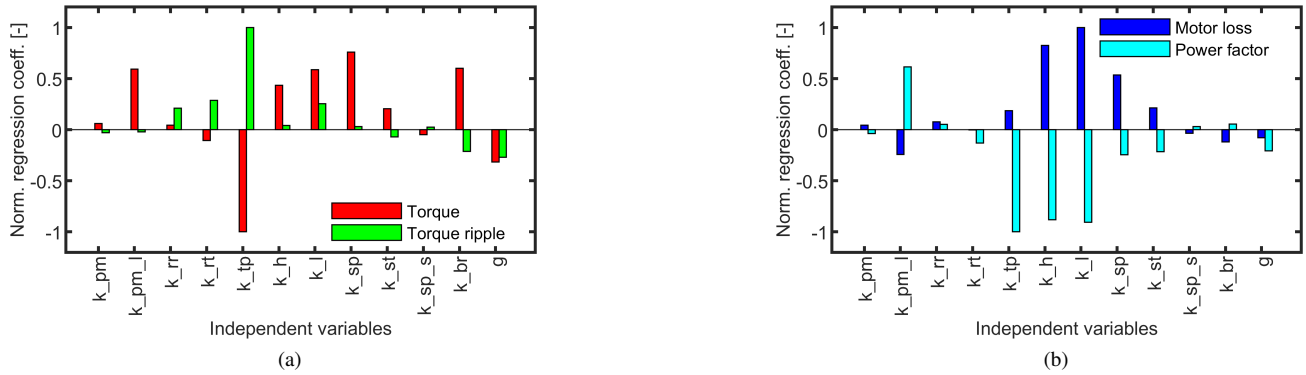

Fig. 6. Normalized non-linear regression coefficients for outer rotor motor configuration showing influence of independent variables on (a) torque and torque ripple, (b) motor loss and power factor, showing a distributed relationship between the variables and studied performance metrics.

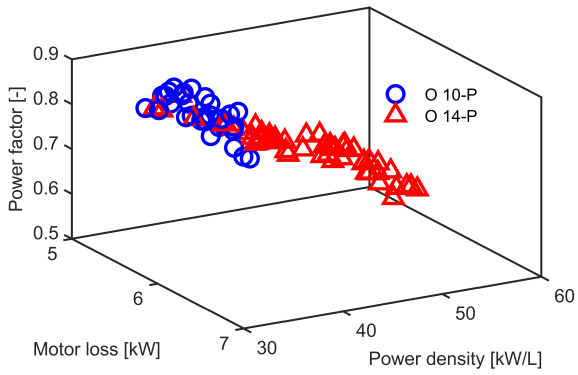

Fig. 7. Pareto front designs for optimization studies of high energy rare-earth versions with 10 and 14 reluctance rotor protrusions.

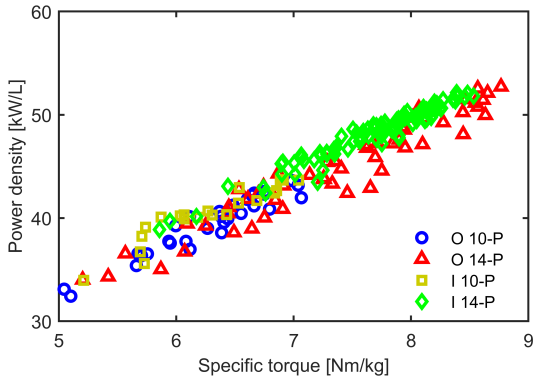

Fig. 8. Comparison of Pareto designs with rare-earth PMs for outer (O) and inner (I) rotor motor topologies with 10 and 14 reluctance rotor protrusions. An active power density higher than 50kW/L is desirable and achievable with 14 pole-pair designs.

The drive cycle performance of an optimal 10″ 28-pole outer rotor motor design "OR-PM D1" employing ferrites as documented in [6] and shown in Fig. 2 is investigated considering application in a light-duty electric vehicle. The reference design has a peak torque of 373Nm at a base speed of 3,000rpm, and its efficiency map as shown in Fig. 10. It is analyzed considering appropriate gear ratios and using seven centroids each for three drive cycles namely the WLTP, the Orange county transit association, and the Parcel delivery truck schedule in Baltimore.

IV. Results and Discussion

A. Comparative Analysis

The DOE-based studies on inner and outer rotor designs highlight key factors influencing torque, torque ripple, motor

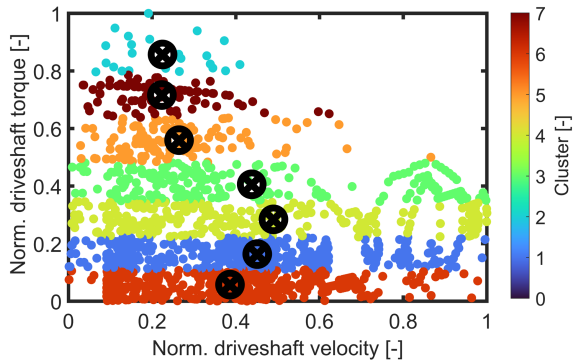

Fig. 9. Torque-speed operating points within the WLTP drive cycle showing the seven centroids which are the most representative as per the k-means clustering.

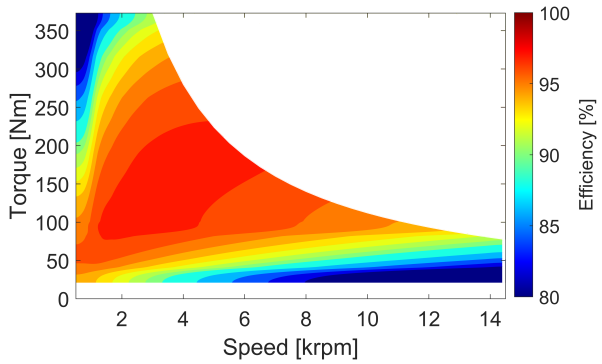

Fig. 10. Efficiency map of OR-PM D1 which is an optimal 10″ 373Nm outer rotor motor design employing ferrites.

Table III
DRIVE CYCLE ANALYSIS FOR THE WLTP REPORTING THE CENTROIDS AND THEIR CORRESPONDING ENERGY WEIGHTS (C.E.W)

Drive shaft			Motor shaft (assuming a gear ratio)			
Cent. no.	Torque [Nm]	Speed [rpm]	Torque [Nm]	Speed [rpm]	C.E.W [-]	Motor eff. [%]
1	978	351	109	3157	0.263	97.3
2	1401	311	156	2796	0.232	97.3
3	553	325	61	2926	0.203	95.8
4	1920	187	213	1687	0.118	95.7
5	2462	163	274	1464	0.093	93.1
6	196	281	22	2529	0.063	91.4
7	2950	159	328	1434	0.029	89.5

loss, and power factor as summarized in Figs. 5 and 6. In the inner rotor design, the split ratio, k_sp, is the most influential factor, such that it must be optimized for a large enough airgap diameter and stator cross-section for optimal torque output. Conversely, the outer rotor design allows for a larger split ratio, offering an advantage for torque within the same volume via the airgap diameter and stator area.

Also, the shaft diameter ratio, k_sh, and stator bridge ratio, k_br, significantly impact torque in the inner rotor design. Reducing the shaft diameter enhances flux linkage and torque by increasing the rotor core, while decreasing the stator bridge ratio provides more room for copper, increasing the torque output for the same current density. This agrees with increased copper area via increase in the AC slot dimensions ratios, k_l and k_h, in the outer rotor design.

Additionally, the inner rotor topology faces challenges accommodating large coil areas, PMs, stator teeth, and rotors, while the outer rotor design seamlessly integrates these features. For improved power factor and torque ripple, the inner rotor design favors larger rotor diameter, thicker magnets, and wider stator teeth with small slots. In the outer rotor topology, significant improvements in torque ripple and power factor can be achieved through independent optimization of rotor or stator profiles while maintaining the split ratio.

The resulting Pareto fronts from the optimization of outer rotor topology are shown in Fig. 7 and indicate that designs with power factor greater than 0.7 are possible. The 10-protrusion designs typically have higher power factors than the 14-protrusion designs, and in line with expectations, a compromise has to be made between power factor and power density. A summary of the optimized results from the Pareto fronts for both inner and outer rotor topologies are shown in Fig. 8. Higher polarity designs are capable of higher power density in both the inner and outer rotor topologies. The outer rotor design of the higher polarity (O 14-P) has the highest power density capability between the two machines.

B. Drive Cycle Analysis

For the drive cycle analysis, the 10″ outer rotor design employing ferrites achieves an efficiency per cycle of 96.2% for the WLTP cycle, shown in Table III, and even better performance in Orange County and Baltimore cycles with efficiencies per cycle of 98.3% and 98.4% respectively.

These "high" efficiency per cycle values obtained will support high overall system efficiency as the motor is integrated with other units for EV applications.

V. CONCLUSION

A systematic comparison was carried out between the inner and outer rotor topologies of the proposed special machines with PM stators. The geometry of the outer rotor topology enables a larger airgap diameter, rectangular stator slots for high slot fill, and integrated cooling within the same volume, which are desirable for high power density while the inner rotor topology may have the advantage in terms of manufacturing due to its more traditional configuration.

The sensitivity analysis based on DoE shows that the split factor is the most influential geometric parameter for an inner rotor topology, while the outer rotor topology which benefits of flux concentration has a more distributed influence between geometry and performance. Comparison of Pareto designs obtained from large-scale multi-optimization show that outer rotor designs with higher polarity, 14-P, can achieve higher power and torque densities when compared with inner rotor designs.

In addition to the rare-earth PM version, an optimal outer rotor design employing ferrites is proposed for three selected drive cycles. High efficiency per cycle values, reaching up to 98%, were achieved for these specific light-duty EV application cycles.

ACKNOWLEDGMENT

This work was supported in part by the VTO DOE, under award no. DEEE0008871. The material presented in this paper does not necessarily reflect the views of DOE. The direct sponsorship of QM Power, Inc. is also gratefully acknowledged, together with additional support from ANSYS Inc., and the University of Kentucky the L. Stanley Pigman Chair in Power Endowment.

REFERENCES

[1] M. Mohammadi, J. Thornburg, and J. Mohammadi, "Towards an energy future with ubiquitous electric vehicles: Barriers and opportunities," *Energies*, vol. 16, no. 17, 2023.

[2] E. Agamloh, A. von Jouanne, and A. Yokochi, "An overview of electric machine trends in modern electric vehicles," *Machines*, vol. 8, no. 2, 2020.

[3] M. H. Severson, R. T. Nguyen, J. Ormerod, and S. Williams, "An integrated supply chain analysis for cobalt and rare earth elements under global electrification and constrained resources," *Resources, Conservation and Recycling*, vol. 189, p. 106761, 2023.

[4] A. Al-Qarni and A. El-Refaie, "Optimum rotor design for rare-earth free high performance traction applications interior permanent magnet motors enabled by iron nitride permanent magnet," in *2023 IEEE International Electric Machines Drives Conference (IEMDC)*, 2023, pp. 1–7.

[5] P. C.-K. Luk, H. A. Abdulrahem, and B. Xia, "Low-cost high-performance ferrite permanent magnet machines in EV applications: A comprehensive review," *eTransportation*, vol. 6, p. 100080, 2020.

[6] O. A. Badewa, A. Mohammadi, D. D. Lewis, D. M. Ionel, S. Essakiappan, and M. Manjrekar, "Optimization of an electric vehicle traction motor with a PM flux intensifying stator and a reluctance outer rotor," in *2023 IEEE Transportation Electrification Conference Expo (ITEC)*, 2023, pp. 1–6.

[7] O. A. Badewa, A. Mohammadi, D. M. Ionel, S. Essakiappan, and M. Manjrekar, "Electric vehicle traction motor with a reluctance outer rotor and a modular stator with AC concentrated toroidal windings and PM or DC wave winding excitation," in *2023 IEEE Energy Conversion Congress and Exposition (ECCE)*, 2023, pp. 3845–3850.

[8] D. Ionel, J. Eastham, and T. Betzer, "Finite element analysis of a novel brushless DC motor with flux barriers," *IEEE Transactions on Magnetics*, vol. 31, no. 6, pp. 3749–3751, 1995.

[9] D. Ionel, D. Jackson, G. Starr, and A. Turner, "Permanent magnet brushless motors for industrial variable speed drives," in *2002 International Conference on Power Electronics, Machines and Drives (Conf. Publ. No. 487)*, 2002, pp. 650–654.

[10] L. Tom, M. R. Khowja, R. Kumar Ramanathan, G. Vakil, C. Gerada, and M. Benarous, "Investigation of slot shape and associated winding configuration for aerospace actuator motor," in *2023 IEEE International Electric Machines Drives Conference (IEMDC)*, 2023, pp. 1–7.

[11] A. Kampker, H. H. Heimes, B. Dorn, F. Brans, and C. Stäck, "Challenges of the continuous hairpin technology for production techniques," *Energy Reports*, vol. 9, pp. 107–114, 2023.

[12] A. Selema, M. N. Ibrahim, and P. Sergeant, "Advanced manufacturability of electrical machine architecture through 3D printing technology," *Machines*, vol. 11, no. 9, 2023.

[13] D. Konovalov, I. Tolstorebrov, T. M. Eikevik, H. Kobalava, M. Radchenko, A. Hafner, and A. Radchenko, "Recent developments in cooling systems and cooling management for electric motors," *Energies*, vol. 16, no. 19, 2023.

[14] W. Sixel, M. Liu, G. Nellis, and B. Sarlioglu, "Ceramic 3-D printed direct winding heat exchangers for thermal management of concentrated winding electric machines," *IEEE Transactions on Industry Applications*, vol. 57, no. 6, pp. 5829–5840, 2021.

[15] N. Simpson, G. Yiannakou, H. Felton, J. Robinson, A. Arjunan, and P. H. Mellor, "Direct thermal management of windings enabled by additive manufacturing," *IEEE Transactions on Industry Applications*, vol. 59, no. 2, pp. 1319–1327, 2023.

[16] A. Fatemi, D. M. Ionel, M. Popescu, Y. C. Chong, and N. A. O. Demerdash, "Design optimization of a high torque density spoke-type PM motor for a formula E race drive cycle," *IEEE Transactions on Industry Applications*, vol. 54, no. 5, pp. 4343–4354, 2018.

[17] P. Han, M. G. Kesgin, D. M. Ionel, R. Gosalia, N. Shah, C. J. Flynn, C. S. Goli, S. Essakiappan, and M. Manjrekar, "Design optimization of a very high power density motor with a reluctance rotor and a modular stator having PMs and toroidal windings," in *2021 IEEE Energy Conversion Congress and Exposition (ECCE)*, 2021, pp. 4424–4430.

[18] M. Rosu, P. Zhou, D. Lin, D. M. Ionel, M. Popescu, F. Blaabjerg, V. Rallabandi, and D. Staton, *Multiphysics simulation by design for electrical machines, power electronics and drives*. John Wiley & Sons, 2017.

[19] *Ansys® Electronics, version 23.2, 2023, ANSYS Inc.*

[20] M. Murataliyev, M. Degano, and M. Galea, "A novel sizing approach for synchronous reluctance machines," *IEEE Transactions on Industrial Electronics*, vol. 68, no. 3, pp. 2083–2095, 2021.

[21] M. Lehr, D. Dietz, and A. Binder, "Electromagnetic design of a permanent magnet flux-switching-machine as a direct-driven 3 MW wind power generator," in *2018 IEEE International Conference on Industrial Technology (ICIT)*, 2018, pp. 383–388.

[22] B. Anvari, H. A. Toliyat, and B. Fahimi, "Simultaneous optimization of geometry and firing angles for in-wheel switched reluctance motor drive," *IEEE Transactions on Transportation Electrification*, vol. 4, no. 1, pp. 322–329, 2018.

[23] A. Mohammadi, O. A. Badewa, Y. Chulaee, D. M. Ionel, S. Essakiappan, and M. Manjrekar, "Direct-drive wind generator concept with non-rare-earth PM flux intensifying stator and reluctance outer rotor," in *2022 11th International Conference on Renewable Energy Research and Application (ICRERA)*, 2022, pp. 582–587.

[24] K.-H. Kim, H.-I. Park, S.-M. Jang, D.-J. You, and J.-Y. Choi, "Comparative study of electromagnetic performance of high-speed synchronous motors with rare-earth and ferrite permanent magnets," *IEEE Transactions on Magnetics*, vol. 52, no. 7, pp. 1–4, 2016.

[25] M. R. Hoyt, G. I. Falcon, C. J. Pearce, R. E. Delaney, T. E. Stevens, E. M. Johnson, T. M. Szenderski, N. R. Sorenson, S. F. Fultz-Waters, M. A. Rodriguez, L. J. Whalen, and T. C. Monson, "Fabrication and characterization of net-shaped iron nitride-amine-epoxy soft magnetic composites," *Frontiers in Materials*, vol. 10, 2023.

[26] M. Masoumi, K. Rajasekhara, D. Parati, and B. Bilgin, "Manufacturing techniques for electric motor coils with round copper wires," *IEEE Access*, vol. 10, pp. 130 212–130 223, 2022.

[27] N. Taran, D. M. Ionel, V. Rallabandi, G. Heins, and D. Patterson, "An overview of methods and a new three-dimensional FEA and analytical hybrid technique for calculating AC winding losses in PM machines," *IEEE Transactions on Industry Applications*, vol. 57, no. 1, pp. 352–362, 2021.

[28] A. Fatemi, D. M. Ionel, N. A. O. Demerdash, D. A. Staton, R. Wrobel, and Y. C. Chong, "Computationally efficient strand eddy current loss calculation in electric machines," *IEEE Transactions on Industry Applications*, vol. 55, no. 4, pp. 3479–3489, 2019.

[29] M. Popescu and D. G. Dorrell, "Proximity losses in the windings of high speed brushless permanent magnet AC motors with single tooth windings and parallel paths," *IEEE Transactions on Magnetics*, vol. 49, no. 7, pp. 3913–3916, 2013.

[30] A. Fatemi, D. M. Ionel, N. A. O. Demerdash, and T. W. Nehl, "Optimal design of IPM motors with different cooling systems and winding configurations," *IEEE Transactions on Industry Applications*, vol. 52, no. 4, pp. 3041–3049, 2016.

[31] Y. Gai, M. Kimiabeigi, Y. Chuan Chong, J. D. Widmer, X. Deng, M. Popescu, J. Goss, D. A. Staton, and A. Steven, "Cooling of automotive traction motors: Schemes, examples, and computation methods," *IEEE Transactions on Industrial Electronics*, vol. 66, no. 3, pp. 1681–1692, 2019.

[32] N. Taran, V. Rallabandi, D. M. Ionel, P. Zhou, M. Thiele, and G. Heins, "A systematic study on the effects of dimensional and materials tolerances on permanent magnet synchronous machines based on the IEEE Std 1812," *IEEE Transactions on Industry Applications*, vol. 55, no. 2, pp. 1360–1371, 2019.

[33] A. Mohammadi, O. A. Badewa, Y. Chulaee, D. M. Ionel, S. Essakiappan, and M. Manjrekar, "Design optimization of a direct-drive wind generator with non-rare-earth PM flux intensifying stator and reluctance rotor," in *2023 IEEE International Electric Machines Drives Conference (IEMDC)*, 2023, pp. 1–6.